

# Simulation of Plastic Deformation Behaviors of Bulk Metallic Glasses with Micro- and Nano-sized Pores

Hong-Ying Zhang and Guang-Ping Zheng

**Abstract** Based on the phase-field model for deformations in bulk metallic glasses (BMG), shear banding in BMG with micro- and nano-sized pores is simulated and the thermo-plastic deformation behaviors are investigated. In the simulations, we use the free-volume concentration  $w_0$  at the pore surface as a measure of the roughness of the pore. We obtain the critical  $w_0$  when shear bands are initiated from the pore surface under different loading conditions. The effect of local heating due to shear banding on the critical  $w_0$  is also quantitatively determined. By considering the heat conduction around pores, shear banding around vacuum pores or pores filled with helium gas are found to be quite different. It is shown that the nano-sized pores act as sinks or sources for shear bands when the pore surfaces are tailored. The simulations indicate that engineering BMG with nano-sized pores is effective in improving their ductility.

**Keywords** Metallic glasses · Shear bands · Phase-field modeling · Nano-sized pores

## 1 Introduction

Bulk metallic glasses (BMG), which are topologically disordered solids without long-range translational order, as seen in crystalline materials, have high fracture toughness, high strength-to-density ratio, good thermal conductivity and corrosion resistance. However, shear deformation always confined in the narrow localized shear zones in BMG makes these outstanding materials not practical in structural

---

H.-Y. Zhang · G.-P. Zheng (✉)

Department of Mechanical Engineering, Hong Kong Polytechnic University, Hung Hom, Kowloon, Hong Kong, China  
e-mail: mmzheng@polyu.edu.hk

application. Thus, a lot of efforts have been made to develop new kinds of BMG exhibiting ductility [1–6]. It has been of great interest that a certain volume fraction of pores are effective in enhancing the plasticity of BMG without much degradation of its mechanical strength, which is demonstrated first in porous BMG or BMG foams with micro-sized pores [7, 8]. Recently it is found that artificially patterned pores on BMG surfaces or in BMG heterostructures could hinder the catastrophic spreading of shear bands during plastic deformations [9–12], especially those pores with sizes below several hundred nanometers [11, 12]. The mechanical properties of the BMG containing micro-sized or nano-sized pores are much related to the concentration of the pores. In particular, the enhanced ductility of BMG comes from the pores acting as powerful stress concentrators as well as multi-axis stress conditions which result in the multiplication of shear bands.

Shear localization, as the only mechanism for the catastrophic failure of glassy alloys, has attracted significant attention. For examples there are various investigations on this issue using conventional continuum mechanics [13, 14], free-volume-exhaustion mechanism [15] and experimental methods [16]. Although those experiments and simulations have captured the shear banding behaviors during the deformation of BMG, few have obtained the details of the strain/stress fields around the shear bands, and the understanding of the deformation mechanisms of these glassy alloys is still incomplete. In particular, though the study on the shear banding and its relations with pores is especially important and valuable in the development of BMG with superior mechanical properties, the understanding of the deformation mechanisms of BMG containing micro- or nano-sized pores is still limited.

In this work, the effects of pores on shear banding in BMG are investigated based on a phenomenological phase-field model, which has been successfully employed for simulation of shear banding, shear-band propagation and branching in conventional BMG [17]. On one hand, how the shear bands interact with the pores and the effects of heat transfer around the pores on shear banding will be elucidated from the simulations. On the other hand, the results can be compared with experimental data available on porous BMG and BMG with patterned pores or arrays of pores. This paper is arranged as follows. In Sect. 2, the phase-field model used for the simulation is described. In Sect. 3, the effect of pores on plastic and thermo-plastic deformations in BMG is systematically investigated in the model system with a micro-sized pore. In Sect. 4, shear banding in BMG with an array of nano-sized pores is elucidated.

## 2 Simulation Methods

According to the atomic-scale deformation mechanism of BMG [17], the free-energy functional of glassy alloys under external loading can be expressed in terms of a local free-energy density  $f(\varepsilon_{ij}, w)$  that is a function of the defect field  $w(\mathbf{r})$  at the local position  $\mathbf{r}$  only, the energy for deviations from spatial uniformity of defect

distribution, and the kinetic energy associated with the local displacement  $\mathbf{u}(\mathbf{r})$ , as follows:

$$F = \int \left\{ f(w, \varepsilon_{ij}) + \frac{\rho}{2} [\dot{\mathbf{u}}]^2 + \frac{\kappa}{2} |\nabla w|^2 \right\} dV, \quad (1)$$

where  $w$  is the normalized local density of deformation defects and  $\rho$  is the mass density of the glassy alloy;  $\varepsilon_{ij}$  is the local strain tensor;  $\kappa$  is the ‘interfacial’ energy between the regions with different densities of deformation defects. And when a crack appears, it becomes the surface energy. The local free-energy density of a metallic glass can be described as [17],

$$f(w, \varepsilon_{ij}) = e[\varepsilon_{ij}] + \frac{a_0}{2} w^2 + \frac{b_0}{3} w^3 + \frac{c_0}{4} w^4 + \left( \frac{a_1}{2} w^2 + \frac{b_1}{3} w^3 \right) (e[\varepsilon_{ij}] - e_0). \quad (2)$$

The coefficients  $a_0$ ,  $b_0$ ,  $c_0$  depend on the energy landscape of deformation defects, independent of the strain. There should exist an energy barrier between the un-activated ( $w = 0$ ) and activated ( $w = 1$ ) states of deformation defects in the undeformed BMG. When  $w$  increases to a critical value  $w_s = 0.8$  under plastic deformation, deformation defects are activated. Deformation defects can also be activated by thermal effects [18]. The deformation defects activated by temperature can be described as shown in Eq. (2) by defining the relation between the coefficient  $a_0$  and the temperature  $T$  as  $a_0 = a' - b'T/T_g$ , where  $T_g$  is the glass transition temperature and  $a'$ ,  $b'$  are constants.  $a_1$  and  $b_1$  are constants which are described below.

Phase-field modeling of shear banding in BMG is based on the free-energy functional  $F$  of a glass alloy under external loading as discussed in detail in Ref. [17]. According to the Ginzburg-Landau formulism, the equations of motions for the displacement field  $\mathbf{u}$  and the scaled field of deformation defects  $w$  are described as follows,

$$\tau_w \frac{\partial w}{\partial t} = - \frac{\delta F}{\delta w} = \kappa \nabla^2 w - (a_0 w + b_0 w^2 + c_0 w^3) - w(a_1 + b_1 w)(e[\varepsilon_{ij}] - e_0) \quad (3a)$$

and,

$$\rho \frac{\partial^2 \mathbf{u}}{\partial t^2} = - \frac{\delta F}{\delta \varepsilon_{ij}} = \mu \nabla \cdot \left\{ \left[ 1 + w^2 \left( \frac{a_1}{2} + \frac{b_1}{3} w \right) \nabla \mathbf{u} \right] \right\}, \quad (3b)$$

where  $\tau_w$  is the characteristic time of activation of these defects under local shear.  $\mu$  is the shear modulus; The strain energy of metallic glass  $e[\varepsilon_{ij}]$  at the elastic limit is defined as  $e_0$ , which is an important physical parameter of BMG.

Moreover, the local heating due to the localized plastic straining can be described by the heat conduction equation,

$$k\nabla^2 T + \beta \frac{\partial Q}{\partial t} = C_p \rho \frac{\partial T}{\partial t}, \quad (4)$$

where  $Q$  is calculated as  $Q = -T(\partial F/\partial T)$  representing the heat related to the generation or annihilation of deformation defects. Therefore  $Q$  is non-zero only near the shear bands in the model system under tensile deformation. Based on energy conservation,  $Q$  could be much closer to the mechanical work if the speed of the shear band is slow. The parameter  $\beta$  is the coefficient representing the percentage of conversion of mechanical work into heat, or the Taylor-Quinney coefficient.  $\beta = 1$  means the adiabatic heating, while  $\beta = 0$  represents isothermal deformation process.  $k$  is the thermal conductivity and  $C_p$  is the heat capacity.

The shear banding and its propagation in BMG can be described by solving Eq. (3a, 3b) assuming adiabatic conditions in BMG. Adding Eqs. (4) to (3a, 3b) can help us to investigate the deformation behaviors when the local heating effect of shear banding is considered. The material properties are listed as follows:  $T_g = 625$  K; the Young's modulus  $E = 95$  GPa; Poisson's ration  $\nu = 0.35$ ; the mass density  $\rho_0 = 6050$  kg/m<sup>3</sup>. The elastic strain limit under uniaxial tension is  $\varepsilon_0 = 0.02$ . The characteristic time of deformation defect activation is  $\tau_w = 0.25$  ns. Another important parameter, the deformation defect activation energy is generally determined by the strain-rate-sensitivity of plastic flow at a different temperature below  $T_g$ . In this work,  $\Delta G$  is chosen as 4.6 eV at  $T = 300$  K for Zr-based BMG, equivalent to the energy barrier for the deformation defects to be activated. The coefficients in Eq. (2) can be described as  $a_0 = 4(2 - T/T_g)\Delta G$ ,  $b_0 = -24\Delta G$ ,  $c_0 = 16\Delta G$ . The aim of choosing  $a_1 = -6$  and  $b_1 = 6$  is to stabilize the activated deformation defect state at  $w = 1$  under plastic deformation.

The boundary condition of Eq. (3a, 3b) at the pore surface is  $w = w_0$ . Assume  $w$  represents the deformation defect density at the pore surface,  $w_0$  between 0 and 1 could be a measure of the roughness of the pore surface. By solving Eqs. (3a, 3b)–(4), shear banding in BMG consisting of pores could be investigated. We consider a Zr-based BMG plate with dimensions of  $10 \times 10 \times 1$   $\mu\text{m}^3$ . Plastic deformations of the model systems with two types of pores are investigated. First, the effect of pores on shear banding in BMG is systematically investigated in a model system with micro-sized pores, as shown in Fig. 1a. The pore diameter is  $r_0 = 1$   $\mu\text{m}$  and the initial crack length is  $l_0 = 0.2$   $\mu\text{m}$ . The results can be compared with experimental data available mostly in porous BMG containing pores with several microns. Second, BMG containing an array of nano-sized pores are employed to investigate how the patterning of the pores could improve ductility, as shown in Fig. 1b.

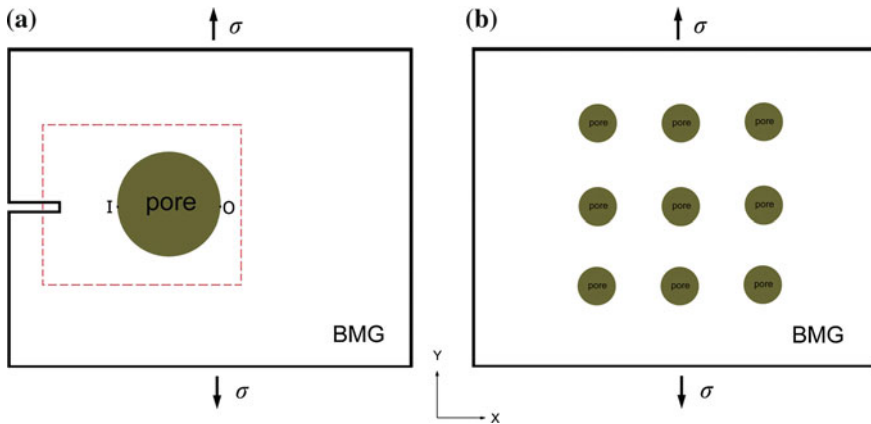


**Fig. 1** **a** Schematic of the model BMG containing a micro-pore. **b** Schematic of the model system containing an array of pores. The length of the initial crack is  $l_0 = 0.2 \mu\text{m}$ . Tensile stress is perpendicular to the initial crack

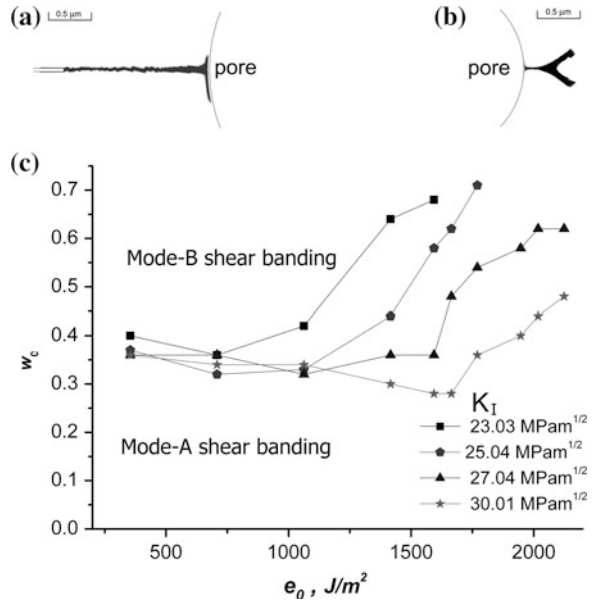
### 3 Simulation of the Effects of Pores on Shear Banding in BMG

#### 3.1 Shear Banding Without Considering Local Heating

We first investigate the interaction between shear band initiated from the initial crack and the pore in BMG without considering local heating. Thus the deformation of BMG is simulated using Eq. (3a, 3b). As shown in Fig. 2a, shear bands generated from an initial crack are discontinuous due to the presence of the pore. From the simulation, it is found that there are two ways that the discontinuous shear band could extend in BMG, as shown in Fig. 2a, b which are denoted as mode-A and mode-B shear banding, respectively. When the pore surface is smooth ( $w_0 \rightarrow 0$ ), shear band is impeded by the pore which has been observed in experiment [8], resulting in mode-A shear banding. When the pore surface is rough ( $w_0 \rightarrow 1$ ), shear band can be initiated from the side of the pore opposite to where the shear band touches the pore, resulting in mode-B shear banding; and the BMG are still brittle. As indicated in Fig. 2a, BMG containing pores could have enhanced fracture toughness if they are deformed via mode-A shear banding.

Stress analyses on mode-A and mode-B shear banding are shown in Fig. 3. In mode-B shear banding, shear stress on the pore surface is heterogeneous. Shear stress tends to build up at the side of the pore surface opposite to where the incident shear band touches the pore; and shear stresses at other places on the pore surface are relaxed as shown in Fig. 3d. The shear band could be initiated at the place marked as 'O' where the stresses concentrate on the pore surface. In mode-A shear banding, shear stresses are built up on several places on the pore surface and are relatively homogeneous as shown in Fig. 3b, and no obvious stress concentration

**Fig. 2** **a** Mode-A shear banding: the shear band is impeded by the pore. **b** Mode-B shear banding: new shear bands are initiated from the pore surface. **c** The critical  $w_0$  (represented as  $w_c$ ) as a function of strain energy at the elastic limit  $e_0$  under different stress intensity factors  $K_I$



can be observed. The stress distribution after the interaction between the incident shear band and the pore can be further revealed by the change of pore geometry under the deformation caused by the stress field of the incident shear band. As shown in Fig. 3c, in mode-B shear banding, the shear deformation of the pore surface is mainly at the side opposite to where the shear band touches the pore, which is marked as ‘O’. Thus shear band could be generated at ‘O’. On the contrary, in mode-A shear banding, shear deformation of the pore surface occurs at its side close to the shear band, which is marked as ‘I’. The shear band is thus impeded by the pore surface near the side marked as ‘I’, as shown in Fig. 3a.

Three factors, the applied tensile stress, the strain energy at the elastic limit of BMG  $e_0$ , and the roughness of the pores  $w_0$ , actually control these modes of shear banding. Under a fixed applied stress, mode-A shear banding changes into mode-B shear banding when the roughness of the pores  $w_0$  changes from 0 to 1, and there exists a critical  $w_0$  represented as  $w_c$  for such a transition of shear banding mode. In Fig. 2c, the  $w_c$  as a function of the strain energy at the elastic limit  $e_0$  is shown for a given applied stress  $\sigma$ . According to the curves shown in Fig. 2c for various stress intensity factors  $K_I = \sigma\sqrt{\pi \cdot l_0}$ , it is seen that  $w_c$  is not significantly affected by  $e_0$  and the applied stress when the strain energy at the elastic limit  $e_0$  is smaller than  $1062 J/m^2$ , and that the critical roughness of the pore surface  $w_c$  is about 0.3–0.4. That means BMG with  $e_0$  smaller than  $1062 J/m^2$  could be tougher if the pore surface is made to have a roughness  $w_0 < 0.3$ , providing an important guideline for the design of BMG containing pores with enhanced fracture toughness.

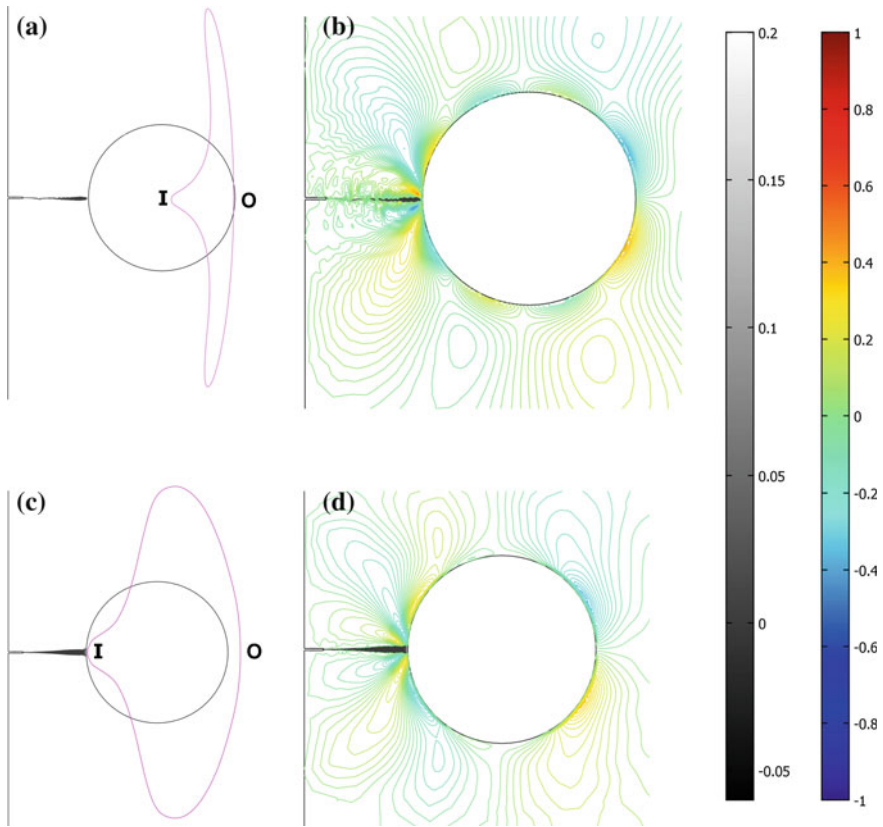


**Fig. 3** **a** Pore surface before (colored in *black*) and after (colored in *pink*) mode-A shear banding. **b** Contour plots of shear stresses in mode-A shear banding. **c** Pore surface before (colored in *black*) and after (colored in *pink*) mode-B shear banding. **d** Contour plots of shear stresses in mode-B shear banding. The *color bar* is for the contour plots of shear stresses. The *gray bar* corresponds to the value of  $1 - w$

### 3.2 The Effects of Heat Conduction Around Pores on Shear Banding

Although in what stage it is relevant to shear banding remains unclear, local heating is an important characteristic of shear banding. In BMG containing pores, local heating could play a dominate role in shear banding since shear bands will be significantly affected by the heat conduction conditions around the pores. For example, shear bands among vacuum pores could be generated by adiabatic deformation, while shear bands around pores filled with gases are formed in a relatively homogeneous thermal environment. To investigate the shear banding by

considering local heating, we solved the coupled Eqs. (3a, 3b)–(4). The initial condition of the heat conduction Eq. (4) is  $T = 300$  K. Other conditions of Eqs. (3a, 3b)–(4) are the same as those in Sect. 3.1.

### 3.2.1 Shear Banding Around Vacuum Pores

In the case that the pores are vacuum holes, it is found that the shear banding modes are related to  $\beta$ , the percentage of mechanical work to heat conversion. Shear banding modes B and C are shown in the insets of Fig. 4. The decreases of  $\beta$  from 1 to 0 change the shear banding from mode C to mode B under a fixed stress intensity factor. In mode-C shear banding, the pore acts as sink and source of shear bands, resulting in shear band multiplication. Hence porous BMG deformed in mode-C shear banding could have better ductility compared with that in mode-B shear banding.

To determine the conditions that BMG containing pores is deformed in mode-C shear banding, we plot diamond symbols in Fig. 4 indicating the critical  $\beta$  (denoted as  $\beta_c$ ) at which mode-B shear banding transforms into mode-C shear banding under different stress intensity factors  $K_I$ . Hence the curve of  $K_I \sim \beta_c$  denotes the boundary of brittle-to-ductile transition, and distinguishes mode-B and mode-C shear banding as discussed above. From Fig. 4 it is remarkable to observe that the adiabatic shear banding ( $\beta \rightarrow 1$ ) results in ductile deformation in porous BMG.

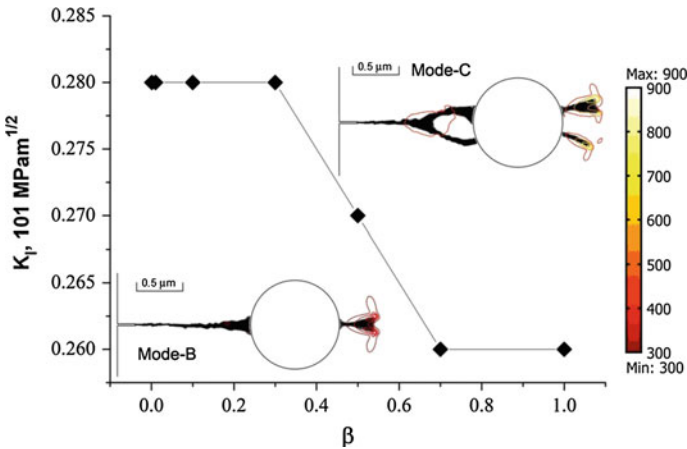


**Fig. 4** Brittle to ductile transition controlled by the coefficient  $\beta$  of mechanical work to heat conversion in porous BMG with vacuum pores. The critical  $\beta$  (denoted as  $\beta_c$ ) at which mode-B shear banding transforms into mode-C shear banding under a stress intensity factor  $K_I$  is plotted as diamond symbol. The color bar is for the contour plots of temperatures. The insets show the brittle porous BMG in mode-B shear banding and the ductile porous BMG in mode-C shear banding



### 3.2.2 Shear Banding Around Pores Filled with Helium

In fact those pores in BMG are usually made by blowing gas bubbles such as helium bubbles into the melts of alloys [19]. Thus the pores could contain gas which provides conduction paths for the heat generated by shear banding around the pores. We consider porous BMG consisting of pores with a diameter of  $1\ \mu\text{m}$ . The pores are filled with helium at 100 kPa which have the physical properties as follows, thermal conductivity  $0.152\ \text{W/m K}$ , heat capacity  $5193\ \text{J/kg K}$ , and density  $0.178\ \text{kg/m}^3$ . The shear banding around pores filled with helium is shown in Fig. 5a–d, assuming  $\beta = 0, 0.001, 0.1, \text{ and } 1$ , respectively. The stress intensity factor is  $K_I = 32\ \text{MPa}^{1/2}$  and surface roughness of the pore is  $w_0 = 0.48$ . While shear banding in BMG with vacuum pores under the same pore surface roughness condition and stress intensity factor  $K_I$  are shown in Fig. 5e–h. Comparing the features of shear banding and the temperature distribution around shear bands which are

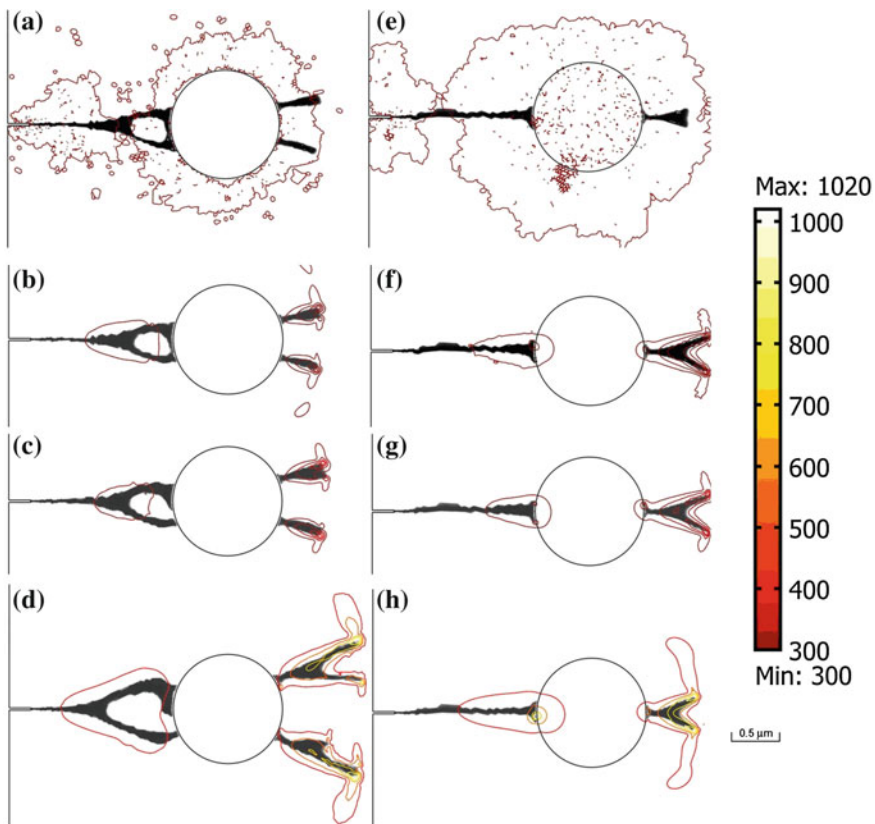


**Fig. 5** Shear banding in BMG with vacuum pores, **a–d**:  $\beta = 0, 0.001, 0.1, \text{ and } 1$ , respectively; and shear banding in BMG with pores filled with helium, **e–h**:  $\beta = 0, 0.001, 0.1, \text{ and } 1$ , respectively. The color bar is for the contour plots of temperatures

close to the vacuum pores and pores filled with helium, we can find that the helium filled in the pores significantly affects the shear banding behaviors in BMG containing pores, while the temperature distribution around shear bands is not much affected. Obviously, BMG containing pores filled with helium deforms in mode-B shear banding and its ductility could be less than that of BMG containing vacuum pores.

#### 4 Plastic Deformation Behaviors of BMG with an Array of Nano-sized Pores

When there are a lot of pores especially those patterned inside BMG, the interaction between the pores and a shear band could be more complicated. As the first attempt in elucidating the plastic deformation of BMG with patterned pores, we consider BMG with a 5-by-5 array of nano-sized pores, as shown in Fig. 1b. The diameter of the pores is 200 nm. A stress  $\sigma$  with  $\sigma\sqrt{\pi \cdot l_0} = 40 \text{ MPa}^{1/2}$  is applied along the Y-direction. Local heating due to shear banding is not considered in the simulation.

Figure 6 shows the shear bandings in BMG with patterned pores whose surface roughness or  $w_0$  varies from 0 to 0.3. Shear bands are initiated from a pore located at the center of the array (denoted as ‘C’) whose surface roughness or  $w_0$  is assumed to be 1. As shown in Fig. 6a, when the pores are smooth ( $w_0 = 0.05$ ) they could effectively block the propagation of shear bands inside the array of pores. The mechanism of such mode-A shear banding has been well discussed in Sect. 3.1. However, an abnormal shear-band multiplication occurs around the site ‘C’ where the shear bands are initiated, as shown in Fig. 6a. Under tensile loading, conventional shear bands generated from the site ‘C’ should propagate along the X-direction perpendicular to the loading direction since the shear stresses close to the site ‘C’ are greatly intensified along the X-direction. As we can observe in the simulation, the conventional shear bands are generated from site ‘C’ along X-direction first. After they are blocked by the pores at the left and right sides of the

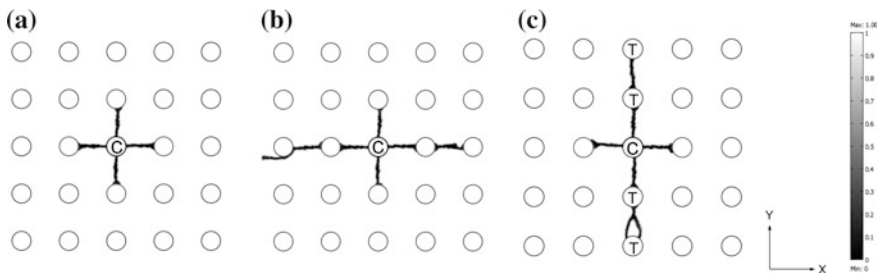


**Fig. 6** Shear banding in BMG with an array of nano-sized pores. **a**  $w_0 = 0.05$ ; **b**  $w_0 = 0.15$ ; **c**  $w_0 = 0.3$  for the pores marked as ‘T’. The rest pores are with  $w_0 = 0.05$ . The nano-sized pores are separated by 1.5  $\mu\text{m}$ . The *gray bar* corresponds to the value of  $1 - w$

site 'C', the shear stresses close to the site 'C' are intensified along the Y-direction, resulting in the generation of abnormal shear bands along the loading direction.

If the roughness of the pores increases, mode-B shear banding could occur. Figure 6b shows a mixed mode-A and mode-B shear banding in BMG with pores whose surface roughness are homogeneous ( $w_0 = 0.15$ ). The abnormal shear banding is still in mode A and blocked by the pores. The simulation results suggest that the plastic deformation of BMG with patterned pores can be controlled by tailoring the roughness of the pore surfaces. Figure 6c demonstrates such an idea that the shear band propagation can be controlled by the pores with heterogeneous surface roughness. If the surface roughness of the pores is  $w_0 = 0.05$  except those marked as 'T', whose surface roughness is  $w_0 = 0.3$ , the abnormal shear banding tends to occur along the pores with large surface roughness. Hence the simulations indicate that engineering BMG with nano-sized pores is effective in improving their ductility.

## 5 Conclusions

Shear banding in BMG containing micro- and nano-sized pores are investigated by phase-field modeling. We find that shear banding in BMG is affected by the surface roughness of the pores, the gas filled in the pores and the elastic limit and Young's modulus of the BMG. The modeling provides quantitative measures on these parameters that determine different modes of shear banding. It is found that the pores act as sinks and sources for shear bands when the BMG containing vacuum pores is deformed in a way similar with adiabatic shear banding, resulting in improved ductility of the BMG. If the pores are filled with gas, BMG may be brittle. The mechanisms of shear banding are found to be consistent with those in BMG consisting of an array of nano-sized pores. The simulations indicate that engineering BMG with nano-sized pores is effective in improving their ductility.

**Acknowledgments** The authors are grateful for the supports provided by the Science and Technology Innovation Commission of Shenzhen and the Research Funds of Hong Kong Polytechnic University (Project No. A-PL98).

## References

1. Schroers J, Veazey C, Johnson WL (2003) Amorphous metallic foam. *Appl Phys Lett* 82: 370–372
2. Wada T, Inoue A (2003) Fabrication, thermal stability and mechanical properties of porous bulk glassy Pd-Cu-Ni-P alloys. *Mater Trans* 44:2228–2231
3. Brothers AH, Dunand DC (2005) Ductile bulk metallic glass foams. *Scripta Mater* 52:335–339
4. Brothers AH, Dunand DC (2005) Processing and structure of open-celled amorphous metal foams. *Adv Mater* 17:484–486

5. Wada T, Inoue A (2004) Formation of porous Pd-based bulk glassy alloys by a high hydrogen pressure melting-water quenching method and their mechanical properties. *Mater Trans* 45:2761–2765
6. Wada T, Inoue A, Greer AL (2005) Enhancement of room-temperature plasticity in a bulk metallic glass by finely dispersed porosity. *Appl Phys Lett* 86:251907
7. Wada T, Inoue A, Greer AL (2007) Mechanical properties of porous bulk glassy alloy prepared in high-pressure hydrogen atmosphere. *Mater Sci Eng A* 449–451:958–961
8. Inoue A, Wada T, Louzguine-Luzgin DV (2007) Improved mechanical properties of bulk glassy alloys containing spherical pores. *Mater Sci Eng A* 471:144–150
9. Sarac B, Schroers J (2013) Designing tensile ductility in metallic glasses. *Nat Commun* 4:2158
10. Kumar G, Tang HX, Schroers J (2009) *Nature* 457:868
11. Lee MH, Sordelet DJ (2006) Nanoporous metallic glass with high surface area. *Scripta Mater* 55:947–950
12. Jayaraj J, Park BJ, Kim DH, Kim WT, Fleury E (2006) Nanometer-sized porous Ti-based metallic glass. *Scripta Mater* 55:1063–1066
13. Stief PS, Spaepen F, Hutchinson JW (1982) Strain localization in amorphous metals. *Acta Metall* 30:447–455
14. Vaks VG (1991) Possible mechanism for formation of localized shear bands in amorphous alloys. *Phys Lett A* 159:174–178
15. Yang B, Morrison ML, Liaw PK, Buchanan RA, Wang G, Liu CT, Denda M (2005) Dynamic evolution of nanoscale shear bands in a bulk-metallic glass. *Appl Phys Lett* 86:141904-1–141904-3
16. Wright WJ, Saha R, Nix WD (2001) Bulk metallic glasses III. Deformation mechanisms of the Zr<sub>40</sub>Ti<sub>14</sub>Ni<sub>10</sub>Cu<sub>12</sub>Be<sub>24</sub> bulk metallic glass. *Mater Trans* 42:642–649
17. Zheng GP, Li M (2009) Mesoscopic theory of shear banding and crack propagation in metallic glasses. *Phys Rev B* 80:104201-1–104201-6
18. Pampillo CA (1972) Localized shear deformation in glassy metal. *Scripta Metall* 6:915–918
19. Wada T, Wang X, Kimura H, Inoue A (2009) Supercooled liquid foaming of a Zr–Al–Cu–Ag bulk metallic glass containing pressurized helium pores. *Mater Lett* 63:858–860